

ISOPHOT OBSERVATIONS OF COMET HALE-BOPP: INITIAL DATA REDUCTION *

E. Grün¹, S. B. Peschke¹, M. Stickel², T. Müller^{2,3}, H. Krüger¹, H. Bönnhardt⁴, T. Y. Brooke²,
H. Campins⁶, J. Crovisier⁷, M. S. Hanner⁵, I. Heinrichsen³, H. U. Keller⁸, R. Knacke⁹,
P. Lamy¹⁰, Ch. Leinert², D. Lemke², C. M. Lisse¹¹, M. Müller^{1,12}, D. J. Osip⁶, M. Solc¹³,
M. Sykes¹⁴, V. Vanysek^{13,+} and J. Zarnecki¹⁵

¹Max-Planck-Institut für Kernphysik, Heidelberg, Germany

²Max-Planck-Institut für Astronomie, Heidelberg, Germany

³ISO Data Center, ESA, Villafranca, Spain

⁴European Southern Observatory, Santiago, Chile

⁵Jet Propulsion Laboratory, Pasadena, USA

⁶University of Florida, Gainesville, USA

⁷Observatoire de Paris, Meudon, France

⁸Max-Planck-Institut für Aeronomie, Katlenburg-Lindau, Germany

⁹Penn State University, Erie, USA

¹⁰Laboratoire d'astrophysique spatiale, Marseille, France

¹¹University of Maryland, College Park, USA

¹²ESA-ESOC, Darmstadt, Germany

¹³Charles University, Prague, Czech Republic

¹⁴University of Arizona, Tucson, USA

¹⁵University of Kent, Canterbury, UK

⁺deceased

ABSTRACT

Comet Hale-Bopp was observed five times with ISOPHOT, the photometer on board the Infrared Space Observatory (ISO). Each time broadband photometry was performed using 4 different detectors, 5 apertures and, 10 filters covering the range between 3.6 to 175 μm . Calibration measurements using the internal Fine Calibration Source were done together with each individual measurement. Background observations were performed with identical instrument settings at the same positions on the sky several days after the comet observations. The observation strategy and the initial data reduction steps are described in some detail and the resulting in-band power values of the Hale-Bopp observations and their uncertainties are derived. Initial reduction of these measurements was performed in 3 steps: (1) processing of raw data by removing instrumental and energetic particle effects, (2) averaging of the individual signals, and (3) determination of the detector responsivities and their uncertainties. The detector signal is determined by two different methods and the best value is chosen. At the present level of processing uncertainties range from 10% to a factor of 3 for the low power levels at short wavelengths. The in-band power levels at different wavelengths varied over 3 orders of magnitude.

*ISO is an ESA project with instruments funded by ESA Member States (especially the PI countries: France, Germany, the Netherlands and the United Kingdom) and with the participation of ISAS and NASA.

1. OBSERVATIONS

Comet Hale-Bopp was a unique target-of-opportunity comet during the lifetime of the ISO satellite. Photometric observations of comet Hale-Bopp were performed with the ISOPHOT instrument (Lemke et al., 1996). The aim of this paper is to describe the observations and the initial data reduction scheme in enough detail in order to understand the present uncertainties of the measurement results. Astronomical interpretation of the results in terms of the spectral energy distribution requires additional color and aperture corrections and will be reported in a separate paper (Grün et al., in preparation). ISO viewing constraints together with the comet's orbital geometry limited the visibility of Hale-Bopp for ISO. Observations were only allowed in the solar elongation range of 60° to 120°. In addition, the Earth had to be at least 24° away from the satellite axis. Further pointing constraints were imposed by the Moon and Jupiter. Because of these constraints, comet Hale-Bopp was only observable for ISO during two periods in spring and autumn 1996 and again in winter 1997. Hale-Bopp's perihelion passage occurred in April 1997.

Within the visibility period of Hale-Bopp the lowest possible background had to be found in front of which the observations were to be performed. The search for the lowest background along the arc of Hale-Bopp's orbit was done in two subsequent steps.

First, a raw selection based on the IRAS all-sky survey (ISSA) plates was performed. 'Dark regions' at 12, 25, 60 and $100\mu\text{m}$ along the cometary track on the ISSA plates were selected. Second, the selected regions were examined with IRSKY (IPAC) to assure that no known point sources were within 5 arcmin of the cometary track, and no prominent (cirrus) structures were visible on the $100\mu\text{m}$ ISSA plates. Also the background estimates for each filter of the ISO observations were derived with IRSKY.

Background subtraction is crucial for photometric measurements but standard simultaneous offset measurements were dismissed because of the extended coma of Hale-Bopp. Instead we introduced so-called 'shadow measurements'. A shadow measurement is the repetition of the Hale-Bopp measurement, called master observation, at the same position on the sky that was tracked in the master observation, at a time when the comet and more importantly the coma had moved away from that sky position. Shadow observations were typically performed about one week after the master observations. For this kind of background measurements we assumed that the seasonal variations of the zodiacal emission are small. Because of scheduling problems the 3rd Hale-Bopp observation was not executed as planned but was delayed by about one month and, therefore, these master and shadow observations are a few degrees apart.

Four different detectors of ISOPHOT (Lemke et al., 1996) were used for the observations (Table 1): detector P1, a Si:Ga-detector for observations up to $16\mu\text{m}$, detector P2, a Si:B-detector for the $25\mu\text{m}$ observations, the C100 camera, a 3×3 -pixel-array of nine Ge:Ga-detectors for 60 and $100\mu\text{m}$ observations, and the C200 camera, a 2×2 array of four stressed Ge:Ga-detectors for the $175\mu\text{m}$ observations. All observations were done in single pointing, single filter absolute photometry mode (AOT P03 and P22), i.e. with a subsequent measurement of the Fine Calibration Source (FCS). Multi-aperture measurements (AOT P04) of comet Hale-Bopp are reported in a companion paper (Peschke et al., 1998).

2. DATA PROCESSING

Processing ISOPHOT data from raw data to meaningful astronomical values is a multi-step process with several decisions to be made that affect the end result. This process is described in some detail in order to get an estimate of the uncertainties of the result, and, to allow other researchers to compare their results with ours. For the initial data reduction - that is described in this paper - the ISOPHOT Interactive Analysis tool (PIA, Gabriel et al. 1997) is used as a baseline. In principal, it takes care of detector and instrumental effects and finally results in in-band power values for each individual comet and background measurement (per detector pixel and per bandpass). The second step that comprises color corrections, corrections for flux deficits due to inaccurate pointing and correct aperture scaling for the distributed coma brightness will be discussed later (Grün et al., in preparation). All these corrections are needed to derive a spectral energy distribution in a standardized aperture over a wide wavelength range.

The five ISOPHOT Hale-Bopp observation sequences reported here comprise 558 individual measurements, counting all object, shadow, and calibration (FCS) measurements at up to 10 wavelengths, some of which were multi-pixel measurements with up to 9 pixels. Each of these measurements had to undergo all initial steps of data processing described below before they were combined into 44 Hale-Bopp and background signal values (Table 1).

During the exposure to an infrared source the ISOPHOT detector output voltage ramps-up with time at a rate that is a function of the infrared flux received by the detector. This voltage is recorded and read-out in preset time steps of $1/128\text{ s}$ to $1/4\text{ s}$. The output voltage is digitized with 12 bits resolution over a dynamic range of about 2.2 V. Normally, before the detector output voltage reaches saturation, after a fixed number of read-outs, the voltage is reset and a new voltage ramp is started. Each individual measurement consisted of 4 to 683 voltage ramps. That way, from 512 to 4096 individual voltage values per measurement were obtained. The individual read-out programs were defined in the observation planning phase dependent on the expected flux levels. Table 1 shows parameters of the different measurements.

The objective of the initial data processing is to derive the flux dependent slope of the voltage ramps [V/s] and to determine the responsivity of the detector. The whole data was reduced homogeneously with PIA version 7.1. At raw data (ERD) level, nonlinearities of the detector response and of the electronic amplification are corrected by using the algorithms provided by PIA. During the whole data reduction process, the default criteria for discarding data points have been applied. In case of only 4 read-outs per ramp, just the two middle data points are left for the slope determination of the ramp.

Next, the effects of high energetic particle hits are removed which cause the signal to display discrete steps of variable amplitudes on top of the linear rise. These glitches are removed in two steps, partly on the raw data level, partly after the determination of the slopes. The slopes of the integration ramps have been determined 1) by first order fits to the ramps (method 1) and 2) by determining the in pairs-differences of subsequent non-destructive read-outs (method 2). By applying the drift recognition algorithm with its default settings, an average signal for the measurement was deduced.

To get confidence in the values derived with these two different methods within PIA, a third independent method was introduced to have an independent handle on the effect of glitch removal as well as on detector drifts. For this, only the non-linearity correction was applied to the raw data and further processing occurred outside PIA. All in pairs-differences were computed, regardless of the type of readout. At this stage, the overall trend in the data, the effect of detector drifts and glitches was clearly visible in the data. Glitches could easily be identified by their distance to the bulk data, based on very good statistics. Next, a myriad algorithm was applied to the data which computed and analyzed the distribution of slope values. A trim fraction was introduced to remove the tails of the distribution that contain mainly glitches. Then the remaining data is analyzed for its

momentum and a stable mean method is applied. The derived value reflects the average signal of the measurement. This value together with the appropriate error is written back into a structure for further processing within PIA.

Method 3 is superior to the previous methods when the measurement comprises only a small number of ramps. We calculate the slopes by all methods in parallel but use method 3 for the final result whenever possible. However, in case the voltage increase per read-out is less than 3 mV method 3 deteriorates because of digitization noise and results from method 1 or 2 are used. Independent of the method by which the average signal slope was derived, the standard reset interval correction is applied, dark current is subtracted and the effect of vignetting is corrected in case of the C detectors.

All the above processing steps are applied both to the object and the subsequent FCS measurements. In an FCS measurement the detector is irradiated by the internal calibration lamp (FCS) and the actual detector responsivity can be determined. However, this method works only reliably when the infrared power onto the detector from the FCS is within about a factor of 3 of the power from the object. The FCS power was set beforehand on the basis of estimates of the object brightness. In case of larger deviations - this was the case in about 2/3 of the measurements - the default responsivity should give more reliable results. The actual and default responsivities sometimes showed large deviations: up to a factor of 3 and more, especially in the case of the very low power values at short wavelengths. In several of these cases the FCS heating power and the corresponding power of infrared radiation were out of the calibrated range. In any case, we use the deviation of the different responsivity values (default, and actual responsivities determined by all three methods) as a measure of the uncertainty of the responsivity and the derived in-band power value. Figure 1 shows the derived in-band power values of the Hale-Bopp

measurements. For a single observation the in-band powers at different wavelengths vary over about 3 orders of magnitudes. Note especially the close similarity of the in-band power values of the 27-SEP-1996 and 7-OCT-1996 observations, except for the value at $175\mu\text{m}$. Due to scheduling problems the positions of the master and the shadow observations were offset by a few degrees which only showed a strong effect at the longest wavelength.

Acknowledgments

Effective support by the ISO Project and ISOPHOT Teams is acknowledged. This research was supported by a DLR grant.

REFERENCES

- Lemke, D., U. Klaas, J. Abolins et al., 1996, ISOPHOT - Capabilities and Performance, A&A, 315, L64-L70
- ISSA, 1994, IRAS All-Sky Survey, IPAC, JPL/Caltec, Pasadena
- IRSKY, 'An Observation Planning Tool for the Infrared Sky' 1995, IRAS All-Sky Survey, IPAC, JPL/Caltec, Pasadena
- ISOPHOT Observers Manual, Issue 2.0, 18 March 1994, edited by Klaas, U., Krüger H, Heinrichsen, I. Laureijs, R. ISO Science Operations Team, Noordwijk, ESA/ESTEC.
- Gabriel, C., Acosta-Pulido, J., Heinrichsen, I. et al., 1997 *Astronomical Data Analysis Software and Systems VI*, A.S.P. Conference Series, Vol. 125, 1997, Gareth Hunt and H. E. Payne, eds., p. 108. 6, 108+.
- Peschke, S. B., Stickel, M., Heinrichsen, I. et al., 1998 First maps of comet Hale-Bopp in the far-infrared, in relation to radial profiles at other wavelengths, this volume

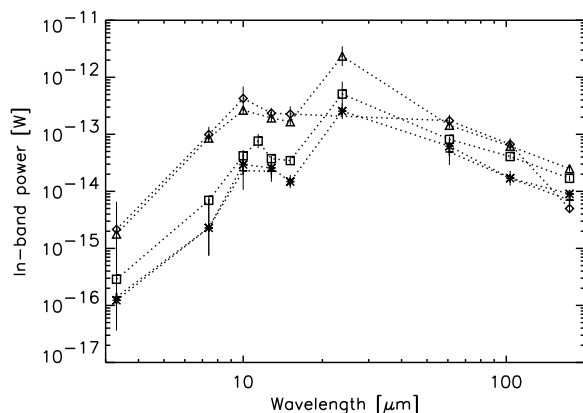


Figure 1. In-band power values of the five Hale-Bopp observations. Different symbols characterise different observations: +: 25-MAR-1996, *: 27-APR-1996, ◇: 27-SEP-1996, △: 7-OCT-1996, □: 30-DEC-1997. Two measurements at $25\mu\text{m}$ wavelengths were not completed because of spacecraft problems.

Table 1. Log of Hale-Bopp and corresponding shadow observations. For each individual ISOPHOT measurement, detector, wavelength of filter, aperture size and integration time are given. For some observations the complete set of filters could not be used. For the specific measurements (Hale-Bopp and shadow) the number of voltage ramps, number of read-outs per ramp and the resulting responsivity and in-band power values are given

Detector	Filter	Aperture size	Integration times	# of ramps	# of read-outs per ramp	Responsivity	In-band power	# of ramps	# of read-outs per ramp	Responsivity	In-band power
	$[\mu\text{m}]$	$['']$	$[\text{s}]$			$[\text{A/W}]$	$[\text{W}]$			$[\text{A/W}]$	$[\text{W}]$
observations				Hale-Bopp, 25-MAR-1996				Shadow, 30-MAR-1996			
P1	3.6	23	256	128	8	1.18	$4.1 \cdot 10^{-16}$	128	8	1.18	$2.7 \cdot 10^{-16}$
P1	7.3	23	32	128	4	1.18	$3.8 \cdot 10^{-15}$	128	4	1.18	$1.5 \cdot 10^{-15}$
P1	10	52	32	128	4	1.18	$2.8 \cdot 10^{-14}$	128	4	1.75	$5.0 \cdot 10^{-15}$
P1	12.8	52	32	128	4	1.18	$2.6 \cdot 10^{-14}$	128	4	3.60	$3.4 \cdot 10^{-15}$
P1	16	52	32	128	4	1.62	$1.5 \cdot 10^{-14}$	128	4	1.18	$6.0 \cdot 10^{-15}$
C1	60	135	32	4	256	70.13	$6.2 \cdot 10^{-14}$	32	32	71.25	$1.3 \cdot 10^{-14}$
C1	100	135	32	4	256	70.51	$2.9 \cdot 10^{-14}$	32	32	54.38	$1.2 \cdot 10^{-14}$
C2	175	180	32	8	128	21.59	$2.5 \cdot 10^{-14}$	16	64	20.59	$1.8 \cdot 10^{-14}$
observations				Hale Bopp, 27-APR-1996				Shadow, 5-MAY-1996			
P1	3.6	23	256	128	8	1.18	$1.5 \cdot 10^{-16}$	128	8	1.17	$2.7 \cdot 10^{-17}$
P1	7.3	23	32	128	4	1.18	$3.0 \cdot 10^{-15}$	128	4	1.17	$7.1 \cdot 10^{-16}$
P1	10	52	32	128	4	1.18	$3.3 \cdot 10^{-14}$	128	4	1.17	$3.5 \cdot 10^{-15}$
P1	12.8	52	32	128	4	1.18	$3.1 \cdot 10^{-14}$	128	4	1.17	$5.2 \cdot 10^{-15}$
P1	16	52	32	128	4	1.53	$1.8 \cdot 10^{-14}$	128	4	1.17	$3.2 \cdot 10^{-15}$
P2	25	99	32	64	32	0.78	$3.0 \cdot 10^{-13}$	128	16	0.64	$4.5 \cdot 10^{-14}$
C1	60	135	32	4	256	32.51	$7.1 \cdot 10^{-14}$	32	32	33.70	$9.1 \cdot 10^{-15}$
C1	100	135	32	4	256	42.49	$2.8 \cdot 10^{-14}$	32	32	33.84	$1.1 \cdot 10^{-14}$
C2	175	180	32	8	128	22.08	$2.4 \cdot 10^{-14}$	32	32	20.55	$1.5 \cdot 10^{-14}$
observations				Hale Bopp, 27-SEP-1996				Shadow, 6-SEP-1996			
P1	3.6	23	256	128	8	1.18	$2.3 \cdot 10^{-15}$	128	8	1.16	$1.5 \cdot 10^{-16}$
P1	7.3	23	32	128	8	1.18	$1.0 \cdot 10^{-13}$	128	4	1.16	$8.8 \cdot 10^{-16}$
P1	10	52	32	128	16	1.18	$4.3 \cdot 10^{-13}$	128	4	1.16	$4.1 \cdot 10^{-15}$
P1	12.8	52	32	64	32	1.18	$2.4 \cdot 10^{-13}$	128	4	1.16	$5.3 \cdot 10^{-15}$
P1	16	52	32	64	32	1.18	$2.3 \cdot 10^{-13}$	128	4	1.16	$3.4 \cdot 10^{-15}$
C1	60	135	32	4	342	38.20	$1.8 \cdot 10^{-13}$	64	16	36.23	$6.5 \cdot 10^{-15}$
C1	100	135	32	4	342	39.54	$8.3 \cdot 10^{-14}$	16	64	31.93	$1.6 \cdot 10^{-14}$
C2	175	180	32	4	256	22.19	$6.1 \cdot 10^{-14}$	16	64	26.52	$5.6 \cdot 10^{-14}$
observations				Hale Bopp, 7-OCT-1996				Shadow, 10-OCT-1996			
P1	3.6	23	256	128	8	1.18	$1.8 \cdot 10^{-15}$	128	8	1.16	$1.9 \cdot 10^{-17}$
P1	7.3	23	32	64	32	1.15	$8.7 \cdot 10^{-14}$	128	4	1.16	$1.1 \cdot 10^{-15}$
P1	10	52	32	32	64	1.18	$2.7 \cdot 10^{-13}$	128	4	1.16	$5.0 \cdot 10^{-15}$
P1	12.8	52	32	32	64	1.02	$2.0 \cdot 10^{-13}$	128	4	1.16	$6.5 \cdot 10^{-15}$
P1	16	52	32	32	64	1.38	$1.7 \cdot 10^{-13}$	128	4	1.16	$3.9 \cdot 10^{-15}$
P2	25	99	32	8	256	0.60	$2.4 \cdot 10^{-12}$	128	16	0.72	$5.2 \cdot 10^{-14}$
C1	60	135	32	4	342	39.29	$1.5 \cdot 10^{-13}$	64	16	36.34	$6.2 \cdot 10^{-15}$
C1	100	135	32	4	342	39.11	$7.3 \cdot 10^{-14}$	32	32	33.07	$1.1 \cdot 10^{-14}$
C2	175	180	32	4	256	22.81	$6.3 \cdot 10^{-14}$	16	64	26.46	$3.8 \cdot 10^{-14}$
observations				Hale Bopp, 30-DEC-1997				Shadow, 4-JAN-1998			
P1	3.6	23	256	128	8	1.18	$2.9 \cdot 10^{-16}$	128	8	1.18	$2.6 \cdot 10^{-18}$
P1	7.3	23	256	128	32	1.18	$7.3 \cdot 10^{-15}$	128	8	1.18	$3.5 \cdot 10^{-16}$
P1	10	52	64	128	32	1.18	$4.4 \cdot 10^{-14}$	128	4	1.18	$2.0 \cdot 10^{-15}$
P1	11.3	52	64	64	64	0.89	$8.1 \cdot 10^{-14}$	128	4	1.18	$4.9 \cdot 10^{-15}$
P1	12.8	52	64	128	32	1.14	$4.0 \cdot 10^{-14}$	128	4	1.18	$2.6 \cdot 10^{-15}$
P1	16	52	64	128	32	1.36	$3.6 \cdot 10^{-14}$	128	4	1.18	$1.4 \cdot 10^{-15}$
P2	25	99	64	16	256	0.76	$5.2 \cdot 10^{-13}$	128	8	0.97	$1.3 \cdot 10^{-14}$
C1	60	135	64	4	683	25.97	$8.3 \cdot 10^{-14}$	64	32	38.49	$1.5 \cdot 10^{-15}$
C1	100	135	64	4	512	32.60	$4.3 \cdot 10^{-14}$	64	32	36.85	$2.2 \cdot 10^{-15}$
C2	175	180	64	16	128	23.25	$2.4 \cdot 10^{-14}$	64	32	24.68	$7.1 \cdot 10^{-15}$